Analysis of the Magnetic Force and the Torque in a Brushless DC Motor

Gunhee Jang* and Dennis K. Lieu**

(Received June 26, 1995)

As permanent-magnet motors and generators produce torque, vibration occurs through the small air gap due to the alternating magnetic forces created by the rotating permanent magnets and the current switching of the coils. The magnetic force can be calculated from the flux density by finite element methods and the Maxwell stress tensor in cylindrical coordinates. The transition of the magnetic force with the rotation of rotor and the commutation of current, was analyzed by assuming the quasi static magnetic field. The cogging and the commutating torques were also investigated by integrating the magnetic shear force in a small air-gap. In addition, the characteristics of these forces and torques were also investigated by multi-dimensional spectral analysis, so that this paper makes it possible to predict the frequency spectrum of magnetic force and the torque in a brushless dc motor.

Key Words : Brushless DC Motor, Magnetic Force, Torque, Vibration, Frequency Spectrum.

Nomenclature

$\boldsymbol{B}$: Magnetic flux density
$\boldsymbol{H}$: Magnetic field intensity
$\boldsymbol{H}_s$: Source magntetic field intensity
L_1 : The period corresponding to tooth angle
L_2 : The period corresponding to rotating angle of the rotor
L_3 : The period corresponding to the torque
R : Distance from the torque center
$\boldsymbol{T}$: Torque
f_i : Traction in i direction
σ_{ij} : Stress
δ_{ij} : Kronecker delta
ω : Rotor speed
θ : Angle
μ : Permeability
Φ : Scalar potential
Y_{km}, X_m, A_k, B_m, Z_n : Complex Fourier coefficient
Ψ_k, Ψ_m, Ψ_n : Fourier shift angle

* Department of Precision Mechanical Engineering, Hanyang University, Seoul, Korea
** Department of Mechanical Engineering, University of California, Berkeley, USA.

1. Introduction

Magnetic force analysis is important in determining not only the torque as the output of motor, but also the source of the vibration in machine itself. Vibration is induced in permanent magnet dc motors and generators as shown in Fig. 1, by traveling magnetic forces. Neodymium and other rare earths have greater retentivity, coercive force and maximum energy product than traditional ferrite magnets. Therefore, since the magnetic force increases approximately with the square of magnetic flux, the forces arising from designs using rare earth magnets are significantly greater than those from conventional magnet designs. These problems are particularly serious when the forcing frequencies match one or more of the structural resonant frequencies in the machine.

The analysis of magnetic force has been addressed by a number of investigators. Initially, papers mainly focused on the calculation of the torque as the output of motor. Reichet et. al. (1976) suggested the finite element method (FEM), the volume integral of the force density and the surface inte-

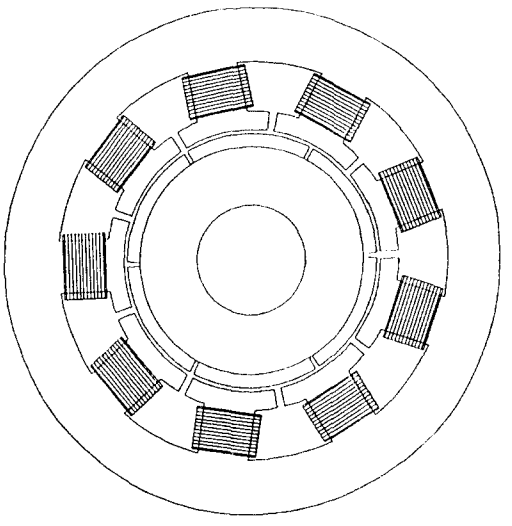

Fig. 1 A dc brushless motor with six poles and nine teeth

gral of Maxwell stress tensor in one single relative position of the movable versus the fixed. Marinescu (1988) and Mizia et. al. (1988) compared the several different method to calculate the torque. Their efforts resulted in torque calculation at several different locations based on the quasi static magnetic field, which were verified by experiments. The problem of magnetically-generated vibreation as a reaction, has been addressed by other investigators. Boules (1985) analytically predicted the flux density in permanent magnet machine. Sabonnadiere et. al. (1989) calculated the magnetic force using the finite element method, while Lefever et al (1989), did so with finite difference method along with determining the dynamic reaction with FEM. Rahman (1991) and Jang (1991) showed that the driving frequencies may be characterized by Fourier decomposition of the magnetic traction, and demonstrated that the vibration levels could be reduced by proper shaping of the magnet. In addition, Jang and Lieu (1992) showed that the composition of the frequency spectrum can be shifted to higher frequencies to reduce the overall transmission to the base system. The transmissibilities of the higher frequencies are low except when the structural resonance occurs. Jang and Lieu (1992, 1993) also reported that the amplitudes of the driving frequencies increase as the pole separation increases. Vibration reduction could be effected by interlacing higher energy magnets and slightly changing the magnetic orientations at the pole transitions or by the interlocking of the magnets.

In this paper, the characteristics of torque and magnetic force acting on the stator was analyzed as the rotation of rotor. This magnetic force in the motor with six poles and nine teeth were calculated from the flux density by finite element methods and the Maxwell stress tensor. Because most motors are driven by the on-off type control, the magnetic force and torque were investigated by two cases, i.e., by the permanent magnet only and by the interaction of the permanent magnet and the current. The components and the characteristics of the magnetic force in a small air gap were analyzed with the introduction of cylindrical coordinate. The transition of this force as the rotation of rotor, was investigated by assuming the quasi static magnetic field. Finally, the frequency spectrum of torque and magnetic force was characterized by the multi-dimensional spectral analysis.

2. Method of Analysis

2.1 Magnetic force and torque

The magnetic field generated by a brushless dc motor is governed by the set of Maxwell's equations. Introducing the scalar potential into the Maxwell equations, with some mathematics, gives a single partial differential equation for the scalar potential.

$$\nabla^T \mu \nabla \Phi - \nabla^T \mu \boldsymbol{H}_s = 0 \tag{1}$$

The field intensity due to the current in the winding and the permanent magnet, may always be calculated directly by the Biot-Savart law and the magnetic dipole moment per unit volume, respectively. This equation, like the Poisson's equation for electrostatic fields, can be solved using the finite element method. TOSCA, a FEM solver for magnetic field, was used to calculate the scalar potential Φ and the magnetic field intensity, $\boldsymbol{H}$.

A non-uniform distributed force per unit area at the interface between two materials is calculated by use of the Maxwell stress tensor. Since the strain imposed on the material due to magnetostriction is small enough to neglect changes in the density, it can be assumed that the change of permeability is negligible. Thus, in tensor notation.

$$\sigma_{ij}=\frac{1}{\mu}\left(B_iB_j-\frac{1}{2}\delta_{ij}B_kB_k\right) \tag{2}$$

where σ_{ij} is the Maxwell stress tensor. B_i is the magnetic flux density which is obtained by the multiplication of permeability to the magnetic field intensity. From the expression given by Woodson and Melcher (1985) for an interface between two materials a and b, the traction, f_i, is given by :

$$f_i=(\sigma_{ij}^a-\sigma_{ij}^b)n_j \tag{3}$$

The normal and the tangential traction can be decomposed.

$$f_n=(\sigma_{ij}^a-\sigma_{ij}^b)n_in_j \tag{4}$$

$$f_t=\sqrt{|f_i|^2-|f_n|^2}=|\boldsymbol{n}\times\boldsymbol{f}\times\boldsymbol{n}| \tag{5}$$

Since $\mu_{\text{air}}\ll\mu_{\text{iron}}$, the magnetic traction can be simplified with the introduction of the cylindrical coordinate on the stator. Along the air gap, the normal and the tangential traction for tooth face are as follows :

$$f_r\approx\sigma_{rr}^a=\frac{1}{2\mu_{\text{air}}}(B_r^2-B_\theta^2-B_z^2) \tag{6}$$

$$f_\theta\approx\sigma_{r\theta}^a=\frac{1}{\mu_{\text{air}}}B_rB_\theta \tag{7}$$

But for tooth side which is perpendicular to the air gap, the normal and the tangential traction have the following form :

$$f_\theta\approx\sigma_{\theta\theta}^a=\frac{1}{2\mu_{\text{air}}}(B_\theta^2-B_r^2-B_z^2) \tag{8}$$

$$f_r\approx\sigma_{r\theta}^a=-\frac{1}{\mu_{\text{air}}}B_rB_\theta \tag{9}$$

The torque produced for one position can easily be derived from the integration of the shear force along the small air gap with the fact that the field distribution inside a closed surface in air remain unchanged if the external sources are removed and replaced by currents and poles on the surface (Reichert et. al., 1976).

$$T=\oint R\times f_\theta d\Omega \tag{10}$$

2.2 Multi-dimensional spectral analysis

The magnetic field produced as the rotor rotates, can be thought of as a series of magnetostatic fields, or quasi-static magnetic fields, with the assumption that the magnetic field produced by the permanent magnets and the current is not significantly affected by the other dynamic effects, such as eddy current and the rise and fall time of current.

The magnetic traction acting on a single tooth and the torque can be interpolated and their frequency components can be determined within the accuracy of the Nyquist sampling theorem by multi-dimensional Fourier transform (Newland, 1984). With the period of L_1 and L_2 corresponding to tooth angle, θ, and rotating angle, ωt, the magnetic traction is

$$f(\theta,\ \omega t)=\sum_{k=-\infty}^{\infty}\sum_{m=-\infty}^{\infty}Y_{\text{km}}\,\boldsymbol{e}^{i2\pi\left[\frac{k\theta}{L_1}+\frac{m\omega t}{L_2}\right]} \tag{11}$$

The complex Fourier coefficient is defined as

$$Y_{km}=\frac{1}{L_1L_2}\int_0^{L_1}d\theta\int_0^{L_2}d\omega t\cdot f(\theta,\ \omega t)\,\boldsymbol{e}^{-i2\pi\left[\frac{k\theta}{L_1}+\frac{m\omega t}{L_2}\right]} \tag{12}$$

Subscript k and m represent the quantities in the frequency domain corresponding θ and ωt. The driving frequencies and their amplitude can be determined by using the Euler identity and decomposing $Y_{km}=A_kB_m$.

$$f(\theta,\ \omega t)=X_0(\theta)+\sum_{m=1}^{\infty}2\cdot X_m(\theta)\cdot\cos(m\omega t+\Psi_m) \tag{13}$$

where X_0 and X_m are the average value and the amplitude corresponding to the frequency component, $m\omega$, and they represent as follows for the stator with nine teeth.

$$X_0(\theta)=Y_{00}+\sum_{k=1}^{\infty}2\,|\,Y_{k0}\,|\cdot\cos(9k\theta+\Psi_k) \tag{14}$$

$$X_m(\theta)=|\,Y_{0m}\,|+\sum_{k=1}^{\infty}2\,|\,Y_{km}\,|\cdot\cos(9k\theta+\Psi_k) \tag{15}$$

where $\Psi_k = \arg(A_k)$ and $\Psi_m = \arg(B_m)$. Magnetic forces acting on other teeth can be easily derived from Eq. (15) by superposing appropriate shift angle to obtain the magnetic force acting on the whole stator.

The period of magnetic force, L_2, is determined by the change of the local force acting on a single tooth. However, the period of torque, L_3, is determined by the change of the global force produced by the integration of the local force on all teeth along the air gap. This illustrates the different frequency spectrum of the magnetic force and the torque. The torque which is obtained by integrating the shear force along the air gap, is

$$T(\omega t) = \sum_{n=-\infty}^{\infty} Z_n \, e^{i\{2\pi \lfloor \frac{n\omega t}{L_3} \rfloor}} \tag{16}$$

$$= Z_0 + \sum_{n=1}^{\infty} 2 \mid Z_n \mid \cdot \cos(n\omega t + \Psi_n) \tag{17}$$

where Z_0 and Z_n are the average value and the amplitude corresponding to the frequency component $m\omega$ and $\Psi_n = \arg(Z_n)$. The complex Fourier coefficient is defined as

$$Z_n = \frac{1}{L_3} \int_0^{L_3} d\omega t \cdot T(\omega t) \, e^{-i2\pi \lfloor \frac{n\omega t}{L_3} \rfloor} \tag{18}$$

3. Finite Element Modeling

Figure 2 shows the finite element model for a brushless dc motor with six poles and nine teeth with the tooth slot and permanent magnet slot modeled on the radial line. The permanent magnet has the residual flux density 1.0 T, coercivity-800 kA/m and the parallel magnetization. The winding of the coil is assumed as a center tapped Y winding, in which the current density (3 A/mm^2) is applied to the coil area (50 mm^2) during the commutation. The rotor would rotate in the counterclockwise direction under the given configuration. Permanent magnet slot and the teeth slot correspond to 2 degree, respectively. Air gap between permanent magnet and the teeth is 1 mm. Because the same geometry with the same orientation of the permanent magnets and the current is repeated every 120 degree, one-third of the model is enough to analyze the whole model with periodicity boundary conditions and it has 43,989 nodes.

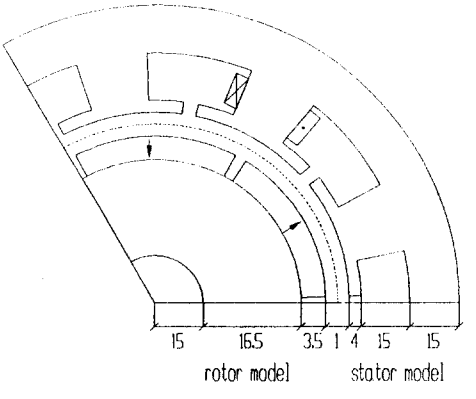

Fig. 2 Finite element model for dc brushless motor

Because the magnetic flux is concentrated in the air gap, particularly at the corner of a tooth, it is necessary to have fine meshes in the air gap and tooth corners in order to have good results. In addition, because magnetic traction is produced by the different permeability of two materials, it is important to determine the magnetic flux density as closely the interface as possible in order to calculate the magnetic force acting on the teeth. The magnetic flux density was determined 0.05mm above the tooth surface. Torque is calculated by integrating the shear traction along the air gap in 35.4mm which produces the smooth curve for the shear traction in order to decrease the integration error.

4. Results and Discussion

4.1 Magnetic flux density and magnetic force

Figure 3 shows the magnetic flux density along the middle tooth of Fig. 2, whose halves face the north and the south pole respectively. Figure 3(a) shows the magnetic flux with no coil current ; i.e., with flux coming from the permanent magnet only. The magnetic flux is distributed in the tooth face and concentrated at the corners of the tooth. B_r exists along the tooth face and at the inner corner of the tooth side and reaches its maximum and minimum values of 1.19 T and -1.19 T at the each end of the tooth face. B_t is 0.2 T and -0.

2 T at the inner corners of the tooth side. B_θ exist only at the corners of the tooth. Its values are 0. 71 T at each end of tooth face, and 0.86 T at each corner of tooth side. Figure 3(b) shows the magnetic flux with the addition of coil current. The current increases the magnetic field in the upper tooth area, which is in the rotation direction, and decreases it in the lower tooth area, which is in the opposite direction under the given configuration. B_r becomes 1.02 T and -1.33 T at each end of tooth face and 0.15 T and -0.28 T at the ends of the lower and the upper tooth side. B_θ, which exists at each end of the tooth face and along the tooth side due to the current, becomes 0. 55 T and 0.85 T at each end of tooth face, and 0.67 T and 1.02 T at the lower and the upper tooth sides, respectively.

Figure 4 shows the magnetic traction corresponding to the configuration in Fig. 3. Figure 4(a) shows the magnetic traction with no coil current. Normal tractions exist on tooth face and the inner corner of tooth side with maximum value of 365 kPa and 138 kPa, respectively. Shear tractions exist only on the corner of tooth due to

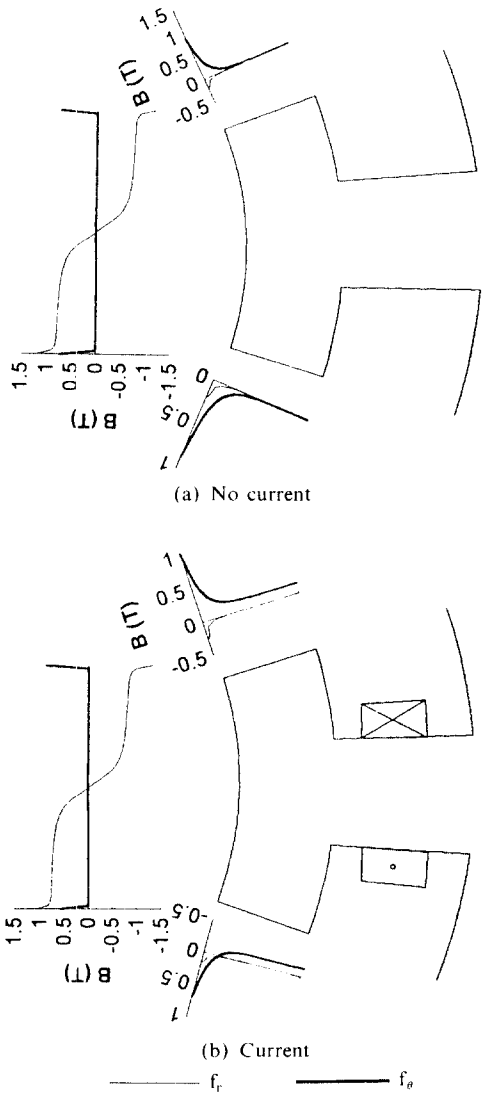

Fig. 3 Magnetic flux density around a tooth

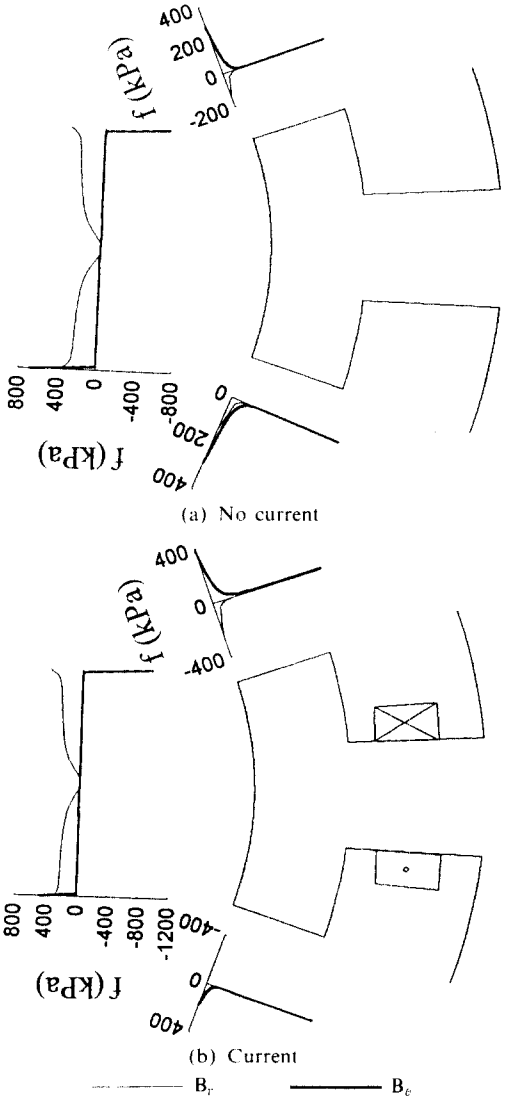

Fig. 4 Magnetic traction around a tooth

the tooth geometry; their maximum values are 680 kPa at the end of tooth face, and 280 kPa at the inner corner of tooth side. Figure 4(b) shows the magnetic traction with coil current applied. Because of the current, magnetic traction in the upper tooth area increases. The normal tractions have 296 kPa and 417 kPa at the lower and the upper end of tooth face, and 84 kPa and -229 kPa at the inner corner of the lower and the upper tooth side. Shear tractions exist mostly on the corner of tooth having values of 457 kPa and -903 kPa at the lower and the upper of tooth face, and 170 kPa and 389 kPa at the inner corner of the lower and the upper tooth side.

The normal tractions are always an attractive tensile force and the orientation of the shear traction is determined by the sign of the product of B_r and B_θ. Figure 5 explains the orientation of the magnetic shear traction acting on the tooth face. In Fig. 5, cases 1 and 2 show the two different positions of poles to the tooth as the rotor rotates. Magnetic flux tends to make a convex curve from the permanent magnet, through the air gap, to the teeth. Its decomposition produces the components of the magnetic flux. In position a and b of Fig. 5, the orientation of the shear traction is positive and negative at each end, respectively, in both case 1 and 2, because the sign of the product of B_r and B_θ is same, even though each sign of B_r and B_θ are different for case 1 and 2. The shear traction on the tooth face is always directed to the adjacent tooth. The shear traction on the tooth side is directed toward the center of the rotor, using the same reasoning. The magnetic tractions around the tooth have the same orientation as shown in Fig. 6, regardless of rotor position and the rotational direction.

The transitions of the magnetic traction acting on the tooth surface with no coil current are shown in Fig. 7. As rotor rotates 120 degree, the polarity and the location of a permanent magnet facing a tooth returns to the original state. Therefore the magnetic force acting on a tooth repeats every 120 degree. In Fig. 7(a) the concentration of the magnetic traction at the ends of tooth face can be observed. The valleys are the result of the permanent magnet slot. In Fig. 7(b), the shear tractions exist only near the ends of tooth face, with a maximum value of approximately 680 kPa. Because of the convexity of the magnetic flux, shear force is negative in the right end (θ=39 degree), and positive in the left end (θ=1 degree) of tooth face regardless of the rotational direction of the rotor and the position of the rotor. The normal and the shear traction on tooth side exist

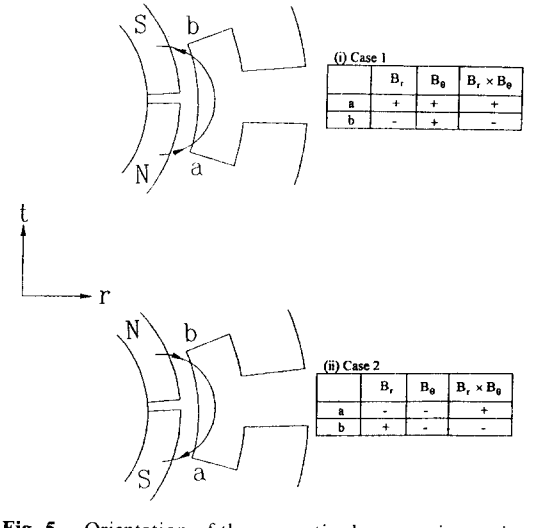

Fig. 5 Orientation of the magnetic shear traction acting on a tooth

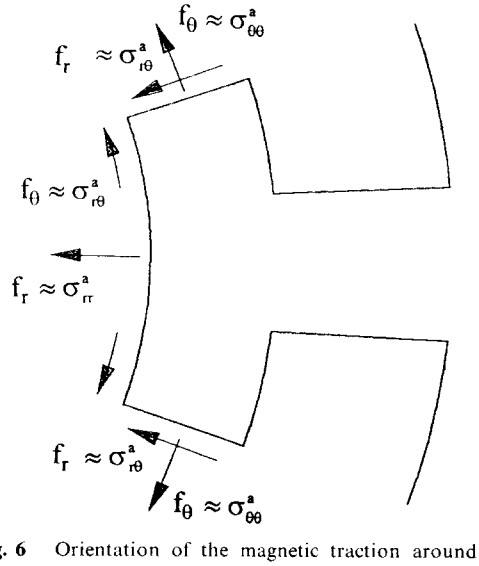

Fig. 6 Orientation of the magnetic traction around a tooth

only on the inside as shown in Figs. 7(c) and (d). Figure 8 shows the transitions of the magnetic traction acing on the tooth surface including a coil current, which increases the magnetic flux in that area. The concentration of the magnetic traction at the right corner ($\theta=39$ degree) of tooth can be observed due to the current, which increases the magnetic flux in that area. The polarity of the permanent magnet and the direction of the current facing a tooth return to the original state as the rotor rotates 120 degree, for the center tapped Y-winding. However, for a center tapped Y-winding brushless dc motor, the current is assumed to commutate at ± 10 degree from the equilibrium position as shown Fig. 2 to maximize the torque output. In Fig. 8(a), the concentration of the magnetic traction at the ends of tooth face, especially at the right end due to the direction of the current, can be observed with the valleys corresponding to the permanent magnet slot. In Fig. 8(b), the shear tractions exist only on the ends of tooth face with a maximum value of appoximately -903 kPa at the right end($\theta=39$ degree). The maximum value at the opposite end of tooth face ($\theta=1$ degree) is 457 kPa. The normal and the shear traction on tooth side exist only on the inside as shown in Figs. 8(c) and 8(d). In Fig. 8, abrupt changes of magnetic trac-

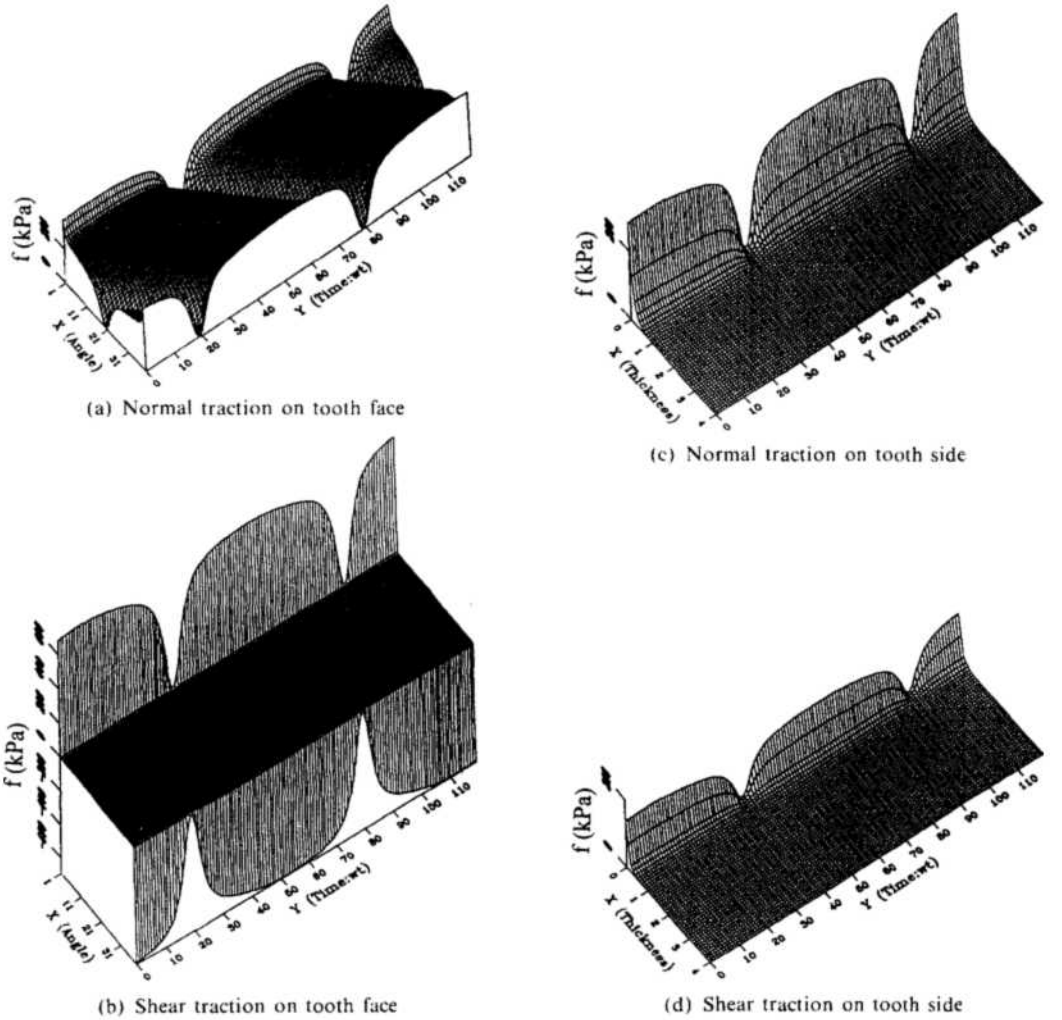

(a) Normal traction on tooth face

(c) Normal traction on tooth side

(b) Shear traction on tooth face

(d) Shear traction on tooth side

Fig. 7 Transition of the magnetic traction with no coil current

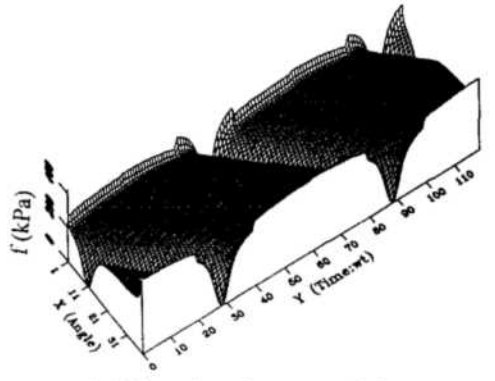

(a) Normal traction on tooth face

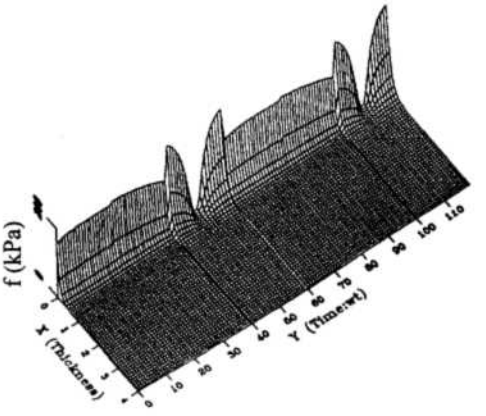

(c) Normal traction on tooth side

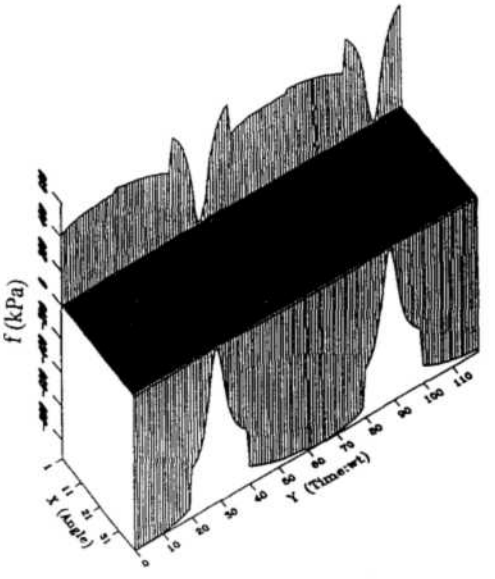

(b) Shear traction on tooth face

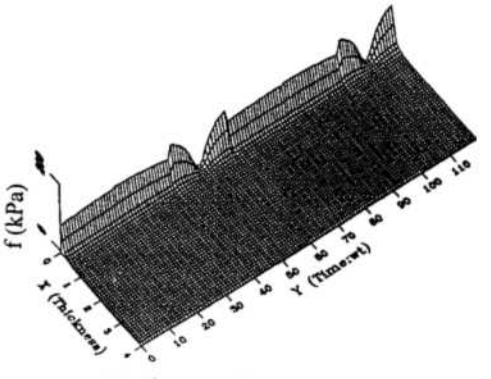

(d) Shear traction on tooth side

Fig. 8 Transition of the magnetic traction with coil current

tion are observed every 20 degree because of the current commutation.

Figure 9 shows the frequency spectrum corresponding to Figs. 7(a) and 7(b). The x-axis corresponds to the subtended angle of tooth, and one degree air gap at each end of tooth. The y-axis represents m frequency component and z-axis shows X_m. All amplitudes(X_m) are zero except those corresponding to every 6th harmonics, which corresponds to the integer multiple of the number of the permanent magnet. As shown in Fig. 9(a), the amplitudes at the corner are larger than those at the other area of tooth face. For example, the amplitude of the 6th harmonic at the corner ($X_6(1)=51.65$kPa) is 28.5% bigger than that at the center of tooth face ($X_6(20)=36.9$ kPa). The amplitude of shear traction are same at each end of tooth face as shown in Fig. 9(b). Even though their amplitudes are much larger than those of the normal traction, they only exist at the each end of tooth face. For example, the amplitude of 6th harmonic of shear traction (94.9 kPa) is 74% bigger than that of normal traction (51.65 kPa). The frequency spectra of the normal and the shear traction on the tooth sides have similar patterns. This magnetic concentration at the corner of tooth which results in the unbalanced magnetic force, excites teeth and produces the

vibration and the noise of motor structure.

Figure 10 shows the frequency spectrum corresponding to Figs. 8(a) and 8(b). Again, all amplitudes are zero except those corresponding to every 6th harmonic, which correspond to the integer multiple of the least common multiple of the number of poles and the number of phase. For six pole and three phase motor, the current commutates every 20 degrees and the current repeats every 60 degrees for the same teeth location ensuring the 6th harmonics. In Fig. 10(a), the amplitudes at each end are different because of the direction of the current. For example, the amplitude of the 6th harmonic at both ends is $X_6(1)=$ 40.4 kPa and $X_6(39)=59.5$ kPa. In Fig. 10(b), the amplitudes of the shear traction are also different at each end of tooth face. For instance, the amplitude of the 6th harmonic at the ends are $X_6(1)=$ 70.0 kPa and $X_6(39)=141.0$ kPa. The frequency spectra of the normal and the shear traction on the tooth sides again have the similar patterns. One important observation is that the current in coil produces the unbalanced magnetic forces at each corner of tooth which excites teeth more severely and generates the vibration and the noise more severly than the case without current.

4.2 Torque generation

The torque produced for one position can easily be derived from the integration of the shear force along the small air gap. Reluctant, or cogging torque is produced only by the magnetic flux

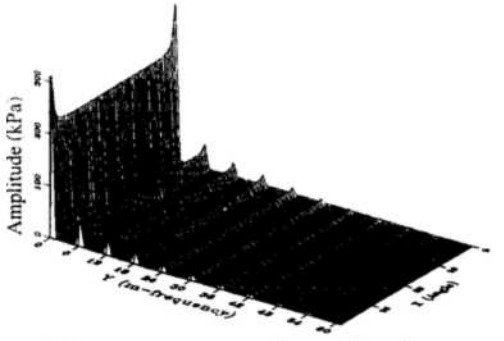

(a) Frequency spectrum of normal traction on tooth face

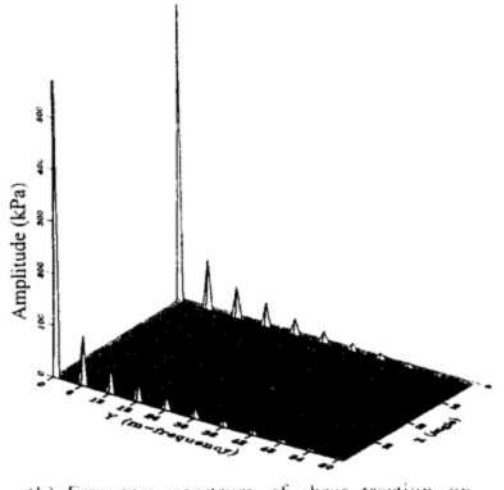

(b) Frequency spectrum of shear traction on tooth face

Fig. 9 Frequency spectra with no coil current

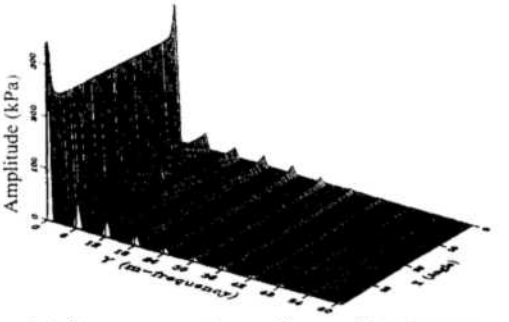

(a) Frequency spectrum of normal traction on tooth face

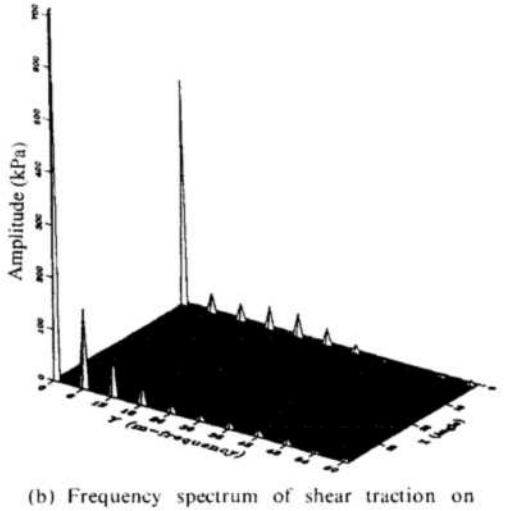

(b) Frequency spectrum of shear traction on tooth face

Fig. 10 Frequency spectra with coil current

from the permanent magnet and the tooth geometry, and tends to move the rotor to the equilibrium position. Figue 11 shows the magnetic flux density and the magnetic traction in the air gap for the equilibrium position. Shear traction is mainly produced in the tooth slot. The shear traction is symmetric, with opposite signs with respect to the center of the tooth slot. Its integration is zero in this equilibrium position. Figure 12 shows the reluctant torque and its frequency spectrum. Even though it has the same relative position of rotor with respect to the stator as rotor rotates 40 degree, torque diagram repeats every 20 degree. Torque is produced by the integration of the shear force, which is governed by the multiplication of B_r and B_θ whose signs change together after 20 degree rotation. This explains the observation that the driving frequency of the reluctant torque is every 18th harmonic of rotation, which is the integer multiple of the least common multiple of the number of poles and the number of teeth.

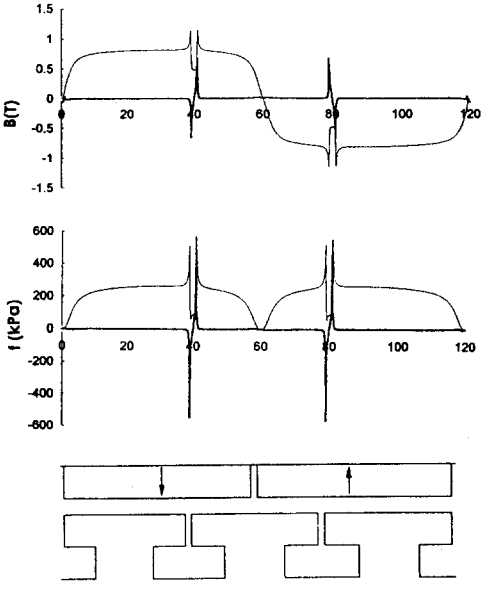

Fig. 11 Magnetic flux density and traction with no coil current

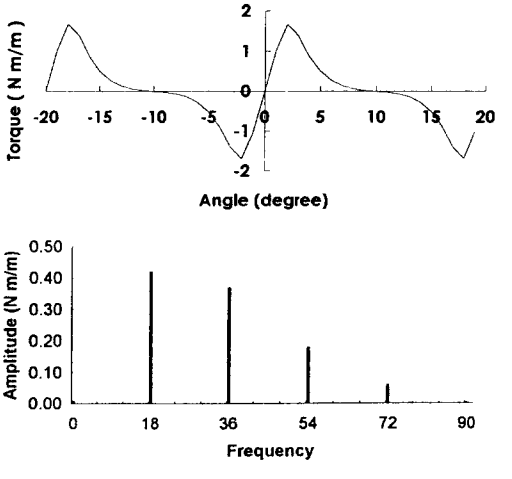

Fig. 12 Reluctant torque and its frequency spectrum

Commutating torque is produced by the interaction between the permanent magnet and the coil current. The current commutates in such a way to turn the rotor in the desired direction. The magnetic flux density and traction in the air gap for the motor with six poles, nine teeth and center tapped Y-winding is shown in Fig. 13. The shear traction has the different distribution with respect to the center of tooth slot. The current increases the shear traction at the left tooth end to rotate the rotor in a counterclockwise direction. Its integration along the air gap produces the commutating torque. Figure 14 shows the commutating torque and its frequency spectrum. Even though the

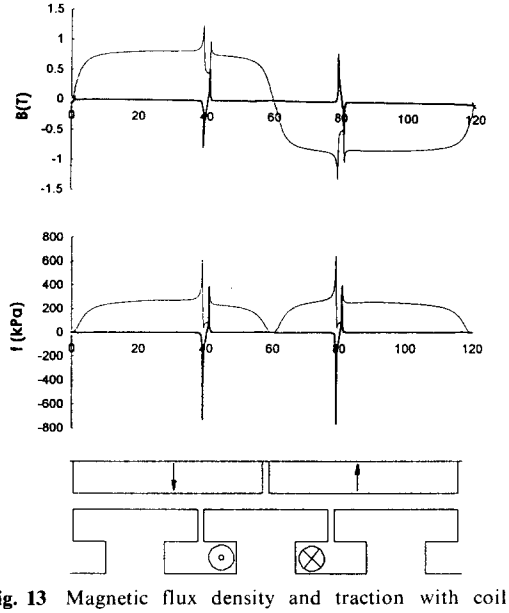

Fig. 13 Magnetic flux density and traction with coil current

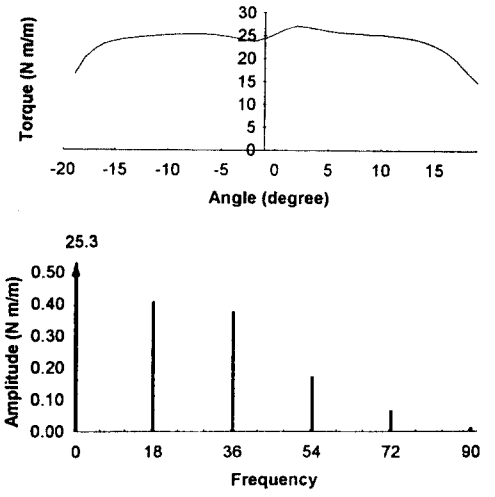

Fig. 14 Commutating torque and its frequency spectrum

possible commutating range is from ± 19 degree as shown in Fig. 14, which produces the positive torque, the maximum torque can be obtained by energizing the central 20 degree. As rotor rotates 20 degree from -10 to 10 degree, the coil in the next right tooth is energized with an opposite current. The magnetic flux pattern facing to it thus has a different direction so that commutating torque repeats for the next 20 degrees. This effect explains the observation that the driving frequency of the commutating torque is also at the 18th harmonic of the rotation frequency of the motor, which corresponds to the integer multiple of the number of poles and the number of phases. Compared with the frequency spectrum of the reluctant and the commutating torque as shown Fig. 12(b) and Fig. 14(b), the difference of the amplitudes of major four harmonics is within 10%, indicating that the reluctant torque is the one of the major source of torque ripple.

5. Conclusion

A method for the analysis of the magnetic force and the torque in a brushless dc motor has been presented from the finite element method, Maxwell stress tensor and multidimensional spectral analysis, so that the characteristics of the magnetic force and the torque can be predictable.

The magnetic forces, especially unbalanced ones with coil current at teeth corner, excite teeth and generate the vibration and the noise. Nomal tensile forces acting on the tooth side as well as the tooth face mainly come from the permanent magnet. The shear forces existing at the end of teeth face, produced by tooth geometry and by the current, always direct toward adjacent tooth slot, and those acting on tooth sides direct toward the center. The driving frequency of the magnetic force is defined by the integer multiple of the rotor speed multiplied by the number of permanent magnet without current, and by the integer multiple for rotor speed multiplied by the least common multiple of the number of poles and the number of phases with current, respectively.

Shear force existing in a small air gap produces the torque. The permanent magnet and the teeth geometry produces the reluctant torque, which increases the magnetic field of the teeth corner with the direction to move the rotor to the equilibrium position. The commutating torque is produced by the interaction of the permanent magnet and the current, which increases the magnetic field concentration of the teeth corner in the moving direction and decreases it in the opposite direction. The driving frequency of the reluctant torque is defined by the integer multiple of the rotor speed multiplied by the least common multiple of the number of poles and the number of teeth. The driving frequency of the commutating torque is defined by the integer multiple of the rotor speed multiplied by the multiple of the number of poles and the number of phases.

References

Boules, N., 1985, "Prediction of No-Load Flux Density Distribution in Permanent Magnet Machines," *IEEE Trans Ind Appl*, Vol. IA-21, No 3, pp. 633~643.

Jang, G. H. and Lieu, D. K., 1991, "The Effect of Magnetic Geometry on Electric Motor Vibration," *IEEE Transactions on Magnetics*, Vol. 27, No. 6, pp. 5202~5204.

Jang, G. H. and Lieu, D. K., 1992, "Vibration Reduction in Electric Machine by Magnet Inter-

lacing," *IEEE Transactions on Magnetics*, Vol. 28, No. 5, pp. 3024~3026.

Jang, G. H. and Lieu, D. K., 1993, "Vibration Reduction in Electric Machine by Interlocking of the Magnets," *IEEE Transactions on Magnetics*, Vol. 29, No. 2, pp. 1423~1426.

Lefevre, Y., Davat, B. and Lajoie-Mazenc, M., 1989, "Determination of Synchronous Motor Vibrations Due to Electromagnetic Force Harmonics," *IEEE Transactions on Magnetics*, Vol. 25, No. 4, pp. 2974~2976.

Marinescu, M. and Marinescu, N., 1988, "Numerical Computation of Torques in Permanent Magnet Motors by Maxwell Stresses and Energy Method", *IEEE Transactions on Magnetics*, Vol. 24, No. 1, pp. 463~466.

Mizia, J., Adamiak, K., Eastham, A. R. and Dawson, G. E., 1988, "Finite Element Force Calculation : Comparison of Methods for Electric Machine," *IEEE Transactions on Magnetics*, Vol. 24, No. 1, pp. 447~450.

Newland, D. E., 1984, *An Introduction to Random Vibrations and Spectral Analysis*, Longman Scientific & Technical, Essex, England, pp. 223~231.

Rahman, B. S. and Lieu, D. K., 1991, "The Origin of Permanent Magnet Induced Vibration in Electric Machines," *ASME Journal of Vibration and Acoustics*, Vol. 113, No. 4, pp. 476~481.

Reichert, K., Freundl, H. and Vogt, W., 1976, "The Calculation of Forces and Torques within Numerical Field Calculation Method," *Proc. COMPUMAG*, pp. 64~68.

Sabonnadiere, J. C., Foggia, A., Imhoff, J. F., Reyne, G. and Meunier, G., 1989, "Spectral Analysis of Electromagnetic Vibrations In D.C. Machines Through the Finite Element Method," *1989 Digests of the 1989 IEEE Intermag Conference*, p. Ec-07.

Trowbridge, C. W., 1990, *An Introduction to Computer Aided Electromagnetic Analysis*, Vector Fields Ltd, Oxford, England.

Woodson, H. and Melcher, J., 1985, *Electromechanical Dynamics*, Part Ⅱ : Fields, Forces, and Motion, The Robert E. Krieger Publishing Company, New York, pp. 445~447.